# Effect of Morphology of Polyaniline Nanomaterials on Cure Kinetics and Properties of Liquid Crystalline Epoxy Nanocomposite

**Joonwon Bae**

*Samsung Advanced Institute of Technology, Yong-In City, Gyeong-Gi Province, Republic of Korea 446-712*

Received 15 February 2011; accepted 20 September 2011
DOI 10.1002/app.36265
Published online 22 December 2011 in Wiley Online Library (wileyonlinelibrary.com).

**ABSTRACT:** Three types of polyaniline (PANI) nanomaterials, nanorods with an average diameter of 30 nm, and nanospheres with average diameter of 30 and 300 nm were synthesized and employed as a curing agent and conducting nanofiller to prepare liquid crystalline epoxy (LCE)/polyaniline nanocomposites. The morphological effect of PANI nanomaterials on the cure behavior of LCE/PANI systems was extensively investigated using dynamic and isothermal differential scanning calorimetry (DSC) analysis. Dynamic DSC results showed that PANI nanorod was a more effective curing agent than nanospheres, because nanospheres retarded cure reaction to some extent compared with PANI nanorods. Isothermal DSC demonstrated that degree of cure was independent of PANI nanoshape. The effect of PANI morphology on the performance of cured LCE/PANI nanocomposites was also examined. Thermogravimetric analysis (TGA) illustrated that the LCE/PANI nanorod system exhibited an enhanced thermal stability than LCE/PANI nanospheres. LCE/PANI nanocomposites showed enhanced electrical conductivity regardless of PANI type compared with conventional epoxy composites ($10^{-5}\sim 10^{-4}$ S cm$^{-1}$). Scanning electron microscopy (SEM) revealed that macrophase separation was not observed in LCE/PANI nanocomposites. PANI nanorods are advantageous for improving the performances of LCE/PANI nanocomposites. © 2011 Wiley Periodicals, Inc. J Appl Polym Sci 125: 562–570, 2012

**Key words:** epoxy; polyaniline; nanorod; nanosphere; morphology; cure behavior; nanocomposite

## INTRODUCTION

In the last few decades, liquid crystalline epoxy (LCE) resins have attracted much interest owing to their unique properties such as high tensile strength, low shrinkage, high adhesion, corrosion and chemical resistance, and dimensional stability. A typical LCE molecule is composed of an aromatic mesogenic group and a reactive oxirane ring, with takes part in the cross-linking reaction. The balance of properties between those of a liquid crystalline polymer and an epoxy resin means that LCE materials can offer a great variety for the application of advanced or high performance nanocomposites.[1–7] To date, cure behavior and properties of LCE have been extensively studied.[8–13]

Polyaniline (PANI) is one of the most important electrically conducting polymers due to its relative high processability, electrical conductivity, and environmental stability. Recently, there has been a considerable interest on the synthesis of PANI nanomaterials owing to their potential applications, such as antistatic coating, corrosion protection, batteries and energy storage, catalysts, and chemical sensors.[14–23]

It is possible to prepare novel electrically conducting composites through the combination of complementary properties of LCE and PANI nanomaterials. The combination of advantageous properties of LCE and PANI nanomaterials can offer an attractive route not only to reinforce LCE matrix but also to introduce new electrical properties based on the enhanced electronic interaction. The proposed applications of this unique material include high performance conducting nanocomposites, antistatic coating, and conducting adhesive. So far, several researches have been reported on the fabrication of various electrically conducting nanocomposite materials using conducting polymer as matrix or nanofiller. Most researches have employed conducting polymer matrix such as polypyrrole, polyaniline, and poly(*p*-phenylenevinylene) or have incorporated inorganic component into polymer matrix.[15,16,24–26] However, limited information is available concerning the fabrication and application of thermoset polymer based conducting nanocomposites.

In this work, three types of novel PANI nanomaterials such as nanorods with an average diameter of

Additional Supporting Information may be found in the online version of this article.

*Correspondence to:* J. Bae (joonwonbae@gmail.com).

30 nm (R30) and nanospheres with average dimensions of 30 (S30) and 300 nm (S300) were synthesized. R30 was prepared by dispersion polymerization. On the other hand, S30 was fabricated by microemulsion polymerization whereas S300 was produced by dispersion polymerization. It is expected that PANI nanomaterials can play roles of both curing agent owing to the free amine groups and conducting nanofiller in the cured composite due to the high electrical conductivity and environmental stability. It seems clear that the morphology of PANI nanomaterials might exhibit a profound effect on the cure behavior and performance of LCE/PANI nanocomposites. Therefore, it is worthwhile to investigate the morphological effect of PANI nanomaterials on the cure behavior and properties of LCE/PANI nanocomposites for development and performance improvement of novel conducting nanocomposites. In addition, shape difference of PANI nanomaterials was elucidated by comparison R30 with S30, and effect of nanosphere diameter can also be verified by comparison between two nanospheres with different diameters.

## EXPERIMENTAL

### Materials

A liquid crystalline epoxy (LCE) resin, diglycidyl ether of 4,4′-dihydroxy-α-methyl stilbene (DGE-DHAMS) was employed as matrix. The synthesis, physical, and chemical properties of the DGE-DHAMS based epoxy resin have been addressed in the literature.[27,28]

Phenol (2.0 mol) and chloroacetone (1.0 mol) are added to a reactor and cooled with stirring. Concentrated sulfuric acid (1.0 mol) is added dropwise to the stirred solution to maintain the reaction temperature. After postreaction at the −10°C, the viscous orange oil product is mixed with deionized water. The oil product is separated then washed with deionized water. After separation, the recovered oil product is added to a beaker with ethanol and stirred to provide a solution. Deionized water is added to the stirred solution and heating is commenced. As the temperature of the mixture increases, the stirred mixture begins to clear. Each time clearing is observed, sufficient deionized water is added to induce cloudiness, followed by continuation of the mixing and heating. The crystalline product is recovered by filtration, washed with deionized water, and then dried. In this way, 4,4′-dihydroxy-α-methylstilbene was prepared. Subsequently, it was mixed with epichlorohydrin (5 mol), deionized water (8.0% by weight of the epichlorohydrin used) and isopropanol (35% by weight of the epichlorohydrin used). Then the mixture was heated with a stirring under a nitrogen atmosphere. Once the 55°C reaction temperature is achieved, sodium hydroxide (0.90 mol) dissolved in deionized water (8 mol) is added dropwise to the reactor slowly to maintain a reaction temperature. After completion of the aqueous sodium hydroxide addition, the stirring is stopped and the aqueous layer which separates from the reaction mixture is pipetted off and discarded. Then, a second solution of sodium hydroxide (0.40 mol) dissolved in deionized water (64 g) is added to the reactor slowly. After the second addition, the recovered reaction mixture is added to a separatory funnel and washed with deionized water. The separated organic layer is washed with deionized water, recovered, and then rotary evaporated under vacuum. The product is recovered as a crystalline off-white solid with an epoxide equivalent weight of 180.[27] When the DGE-DHAMS resin slowly cool from a melting temperature of 130°C to temperatures between 95 and 56°C, nematic LC domains will form as demonstrated by dynamic DSC.[28] The tensile storage modulus of cured resin was in the range of 600–900 MPa while flexural modulus was approximately 130 MPa.[28]

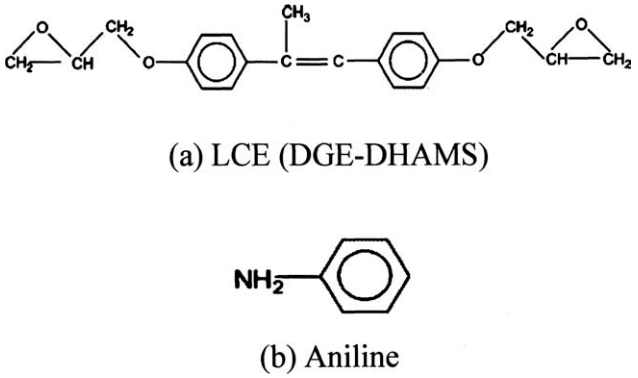


**Figure 1** Chemical structures of LCE and aniline: diglycidyl ether of 4,4′-dihydroxy-α-methyl stilbene; (b) aniline.

The chemical structures of LCE and aniline are displayed in Figure 1. Aniline monomer (ANI), cationic surfactant (decyltrimethylammonium bromide, DeTAB), iron (III) chloride ($FeCl_3$), and initiator (ammonium persulfate, APS) were purchased from Aldrich (Milwaukee, WI, USA) and used as received. Solvents were dried by a common method.

### Synthesis of PANI nanomaterials

PANI nanospheres with an average diameter of 30 nm (S30) were prepared by low temperature microemulsion polymerization. Cationic surfactant (DeTAB, 1.8 g) was dissolved in 20 ml of distilled water at 5 °C and stirred with 200 rpm magnetic stirring for 1 h. Then, 0.5 g of aniline monomer was added dropwise to the surfactant solution. Subsequently, 0.5 g of ammonium persulfate (APS) and

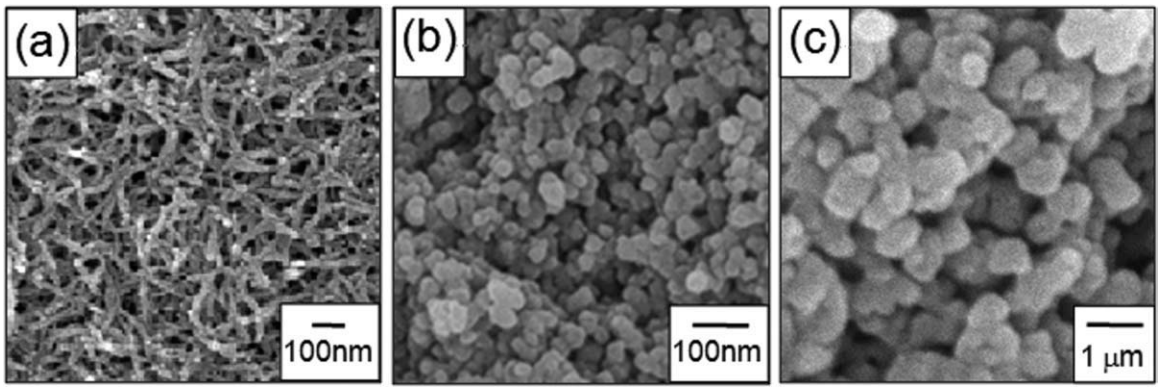


**Figure 2** Scanning electron microscopy images of PANI nanomaterials: (a) PANI nanorods with average size of 30 nm (R30); PANI nanospheres with an average diameter of (b) 30 nm (S30) and (c) 300 (S300) nm.

5 g of 1*M* hydrochloric acid (HCl) were added to the surfactant solution and mixed for additional 1 h. Microemulsion polymerization proceeded for 3 h at 5°C. The surfactant and initiator were removed by excessive amount of ethanol (100 mL, twice) and the PANI precipitates were retrieved and dried in a vacuum oven at 70°C overnight. The yield of S30 was higher than 50%.

On the other hand, PANI nanorod with an average diameter of 30 nm (R30) was synthesized by dispersion polymerization. In a typical procedure, 20 mL of 35 wt % HCl and 2.0 g of aniline were dispersed in 200 mL of distilled water. Then, 4.8 g of APS was added into the solution. Subsequently, 3.75 g of iron (III) chloride was also used for the formation of PANI nanorod. The polymerization of PANI proceeded with magnetic stirring for 3 h. Excessive ethanol (400 mL, 3 times) was added into the resulting product solution to remove the residual HCl, APS, and $FeCl_3$. The upper solution was discarded and the remaining product was dried in vacuum oven overnight at 45°C. PANI nanospheres with an average diameter of 300 nm (S300) were also synthesized by dispersion polymerization without $FeCl_3$. In this case, 10 mL of 5*M* HCl was added as dopant in the polymerization medium. The yields of R30 and S300 were higher than 75%. The average diameter of nanosphere and nanorod was estimated with the assistance of computer software.

### Preparation of sample mixtures for cure

Sample mixtures were prepared by dissolving the LCE and PANI nanomaterials (25% by weight of DGE-DHAMS used) in acetone and sonicating the mixtures for 30 min. Then the solvent was evaporated. The weight ratio of PANI in the sample mixtures was adjusted from 1 to 25 wt % by varying the feeding amount of PANI. The sample mixtures were cured at 175°C for 3 h and post-cured at 190°C for additional 1 h. The mixture composed of LCE and PANI nanorod with an average diameter of 30 nm was designated as R30. LCE mixed with nanospheres of 30 and 300 nm were denoted as S30 and S300, respectively.

### Instrumental analysis

The dynamic differential scanning calorimetry experiments were conducted with a Texas Instrument DSC2920 at heating rates of 2.5, 5, 10, and 20°C/min. The heat of cure was calculated from the integration of area under the cure thermogram. The isothermal DSC experiments were performed in the temperature range of 160–200°C. Below the range, the curing rate is too low to detect the cure reaction, whereas a small amount of thermal degradation occurs over the range. Infrared spectra were obtained by a Bomem MB100 Fourier Transform Infrared (FT-IR) spectrometer. Thermogravimetric analysis (TGA) was conducted with a Perkin Elmer TGA7 at a heating rate of 10°C/min under nitrogen atmosphere. The electrical conductivity of cured samples was measured by the standard four-probe method with Keithley 2400 sourcemeter under ambient conditions.[29] TEM analysis was performed with a JEOL JEM-200CX transmission electron microscope. SEM images were obtained with a JEOL 6700 scanning electron microscope. The EDX analysis was carried out using a JEOL JSM 5410 LV energy dispersive X-ray spectrometer.

## RESULTS AND DISCUSSION

### Polyaniline nanomaterials

Figure 2(a) provides scanning electron microscopy image of PANI nanorods with an average diameter of 30 nm prepared by dispersion polymerization. Two PANI nanospheres with an average diameter of 30 and 300 nm produced by microemulsion and dispersion polymerization were exhibited in

**TABLE I**
**Atomic Composition of Carbon (C) and Nitrogen (N) in PANI Nanorods and Nanospheres**

| PANI nanomaterials | C | N | N/C |
|---|---|---|---|
| R30 | 57.8 | 11.6 | 0.17 |
| S30 | 61.4 | 10.7 | 0.173 |
| S300 | 65.0 | 11.9 | 0.177 |

Figure 2(b,c), respectively. The average size of PANI nanomaterials showed little size distribution. It can be inferred from the images that the molecular weights of PANI nanomaterials also exhibited a narrow distribution; thus the effect of molecular weight distribution on cure kinetics and performance of individual LCE/PANI system was insignificant.[30] The aggregation and deformation of PANI nanomaterials was not observed in the microscopic images. In addition, the atomic compositions of PANI nanomaterials determined with elemental analysis (EA) exhibited the presence of carbon (C) and nitrogen (N). Since an aniline has one nitrogen (N) and six carbons (C), N/C atomic ratio is approximately 0.16–0.18. EA data in Table I exhibited that the N/C composition of PANI nanomaterials were 0.170 (R30), 0.173 (S30), and 0.177 (S300), which were consistent with the N/C ratio of bulk PANI. Energy dispersive X-ray (EDX) spectroscopy indicated the presence of traces of iron (Fe), chlorine (Cl), and sulfur (S) in three types of PANI nanomaterials. This fact confirmed the complete removal of residues such as surfactant and initiators from PANI nanomaterials after washing. The electrical conductivities of PANI nanomaterials were evaluated to be 10.9 S/cm (R30), 5.0 S/cm (S30), and 7.5 S/cm (S300), respectively. Because the electrical conductivity showed very similar values, the effect of electrical conductivity on the performance of resulting nanocomposites might be of little importance.

Figure 3 represents the FT-IR spectrum of PANI nanorods (R30), which shows the vibrational bands 1483 and 1567 $cm^{-1}$ associated with quinoid and benzenoid structures of PANI. The peaks at 1246 and 1300 $cm^{-1}$ were attributed to C—H stretching from aromatic conjugation. These characteristic vibrational bands of PANI were also observed in the spectra of two kinds of PANI nanospheres, S30 and S300. This fact indicates the successful polymerization of aniline by microemulsion or dispersion polymerization.

## Cure behavior

Figure 4 illustrates the FT-IR spectra obtained before and after cure reaction of R30 mixture system. The peak for symmetric C—O—C stretching was observed at 1260 $cm^{-1}$, while that of asymmetric stretching appeared at 912 $cm^{-1}$. The vibrational band at 784 $cm^{-1}$ was assigned to the epoxy half-ring stretching. As the cure reaction between LCE and PANI proceeded, the intensities of these bands decreased due to the epoxide ring opening reaction. To calculate the degree of cure (degree of conversion), the absorption intensity of the peak at 784 $cm^{-1}$ was separated and integrated using Gaussian curve-fitting method. The degree of cure was evaluated to be 0.65. This value was similar to the value (0.70) obtained when the LCE resin was cured with conventional curing agent (sulfanilamide).[29] All these facts confirm that the LCE resin was cured by PANI nanorods, which means that PANI nanomaterials can be employed as a curing agent owing to the surface amine groups. At this condition, the PANI content was 25 wt %. Below this concentration, the curing reaction appeared imperfect judged by external appearance (stayed viscous). Above this content, the occurrence of PANI aggregation might worsen the cure behavior of LCE molecules.

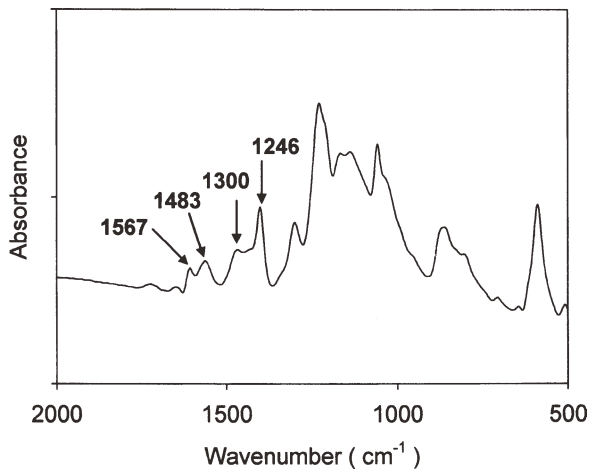


**Figure 3** FT-IR spectrum of PANI nanorods prepared by dispersion polymerization.

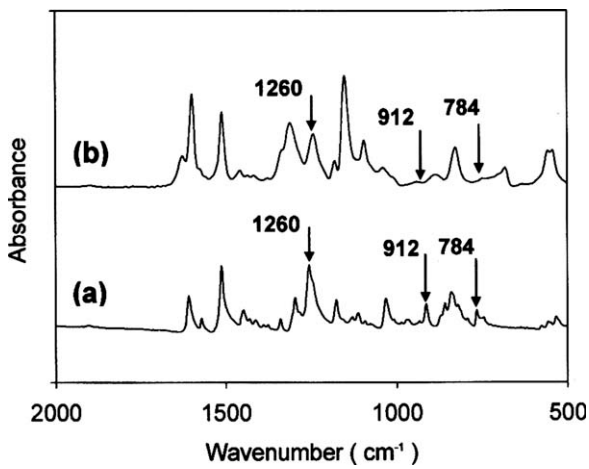


**Figure 4** FT-IR spectra of R30 (25 wt % PANI) system obtained (a) before and (b) after cure reaction.

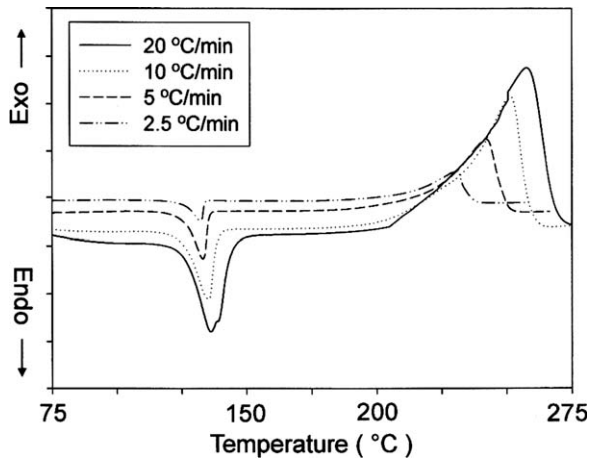


**Figure 5** Dynamic DSC thermograms of S30 (25 wt % PANI) system as a function of heating rate.

The dynamic DSC thermograms of the S30 system are represented in Figure 5 as a function of heating rate. R30 and S300 systems also exhibited similar type of dynamic DSC curves (Supporting Information Fig. S1). Table II summarizes the maximum peak temperature, heat of cure, and activation energy of LCE/PANI systems as a function of heating rate. The activation energies of LCE/PANI systems were calculated using Ozawa equation:[31,32]

$$\log \varphi = C - 0.4567\ E_a/RT_p$$

where $\varphi$ is the heating rate, $E_a$, the activation energy, $T_p$, the peak temperature, and $C$ a constant derived by extrapolation. Activation energy can be calculated from the slope of log $\varphi$ vs. $1/T_p$. The peak temperature and the initial cure temperature increased slightly with increasing heating rate in every system as shown in Table II. For most DSC experiments, the temperature lagging always happens between thermocouple and real samples. The degree of temperature lagging is proportional to the heating rate. Therefore, the peak temperature and the initial cure temperature tend to appear at slightly higher temperature under fast heating condition. The heat of cure was almost independent of the heating rate. However, the heat of cure was dependent on the kind of PANI nanomaterials. This phenomenon was attributed to the morphological difference of PANI nanomaterials. We have explained in a previous paragraph that the effect of molecular factors such as molecular weight and its distribution and molecular structure was insignificant because each PANI nanomaterial showed little size distribution and structural anisotropy (Fig. 2). The heat of cure for R30 system was higher than those of S30 and S300, which meant that PANI nanorods retarded the cure reaction less than PANI nanospheres because the heat of cure is proportional to the extent of cure reaction. In addition, the $E_a$ for R30 was lower than those of S30 and S300. These are because the cure reaction was promoted in the case of R30 owing to the induced orientation of LCE molecules on the surface of PANI nanorods. It has been revealed that the orientation of LCE molecules on the surface of fiber-type materials was promoted, when the fiber-type materials were introduced as filler.[33,34] Therefore, the orientation of LCE molecules on the surface of PANI nanorods can be expected. In this case, chances for LCE-amine complex formation increased and cure reaction occurred fast on the surface of PANI nanorods. This led to the elevation of cure rate and degree of cure. On the other hand, the heat of cure for S30 was higher than that of S300 while the $E_a$ for S30 was lower than that of S300. Because the S30 has a higher surface area than S300, S30 provided more reaction site than S300. The cure reaction around S30 was facilitated due to the increased epoxide-amine interaction owing to the high surface area. In addition, S300 induced more steric congestion than S30 because S300 restricted molecular motion of molecules more than S30 during cure.[35] However, a drastic decrease in the heat of cure was not observed in every LCE/PANI system, which demonstrated that the PANI nanomaterials did not act as a heat-sink during the cure reaction. Judging from the dynamic DSC results, it is clear that PANI nanorod is more useful for cure reaction than PANI nanospheres.

**TABLE II**
**The Peak Temperature ($T_p$), Heat of Cure, and Activation Energy of ($E_a$) LCE/PANI Systems as a Function of Heating Rate**

| System | Scan rate (°C/min) | 20 | 10 | 5 | 2.5 |
|---|---|---|---|---|---|
| R30 | $T_p$ (°C) | 212.9 | 200.1 | 192.7 | 182.3 |
| | Heat of cure (kJ/mol epoxide) | 129.1 | 126.4 | 127.3 | 125.4 |
| | $E_a$ (kJ/mol) | | 116.6 | | |
| S30 | $T_p$ (°C) | 237.2 | 231.5 | 222.8 | 211.4 |
| | Heat of cure (kJ/mol epoxide) | 115.9 | 118.6 | 115.7 | 113.4 |
| | $E_a$ (kJ/mol) | | 135.8 | | |
| S300 | $T_p$ (°C) | 265.6 | 251.8 | 248.7 | 239.5 |
| | Heat of cure (kJ/mol epoxide) | – | 100.6 | 95.9 | 98.5 |
| | $E_a$ (kJ/mol) | | 160.6 | | |

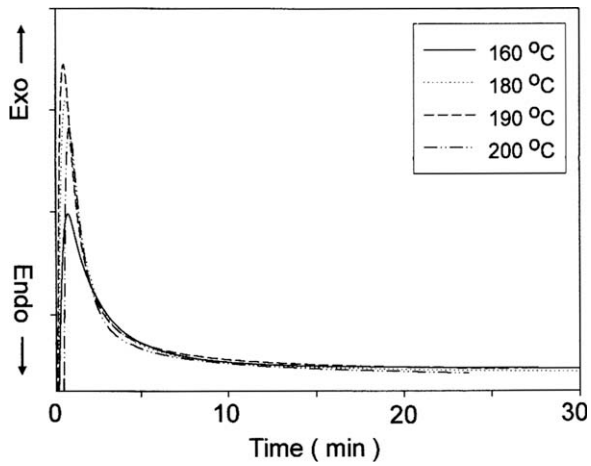


**Figure 6** Isothermal DSC curves of S300 (25 wt % PANI) system as a function of cure temperature.

The isothermal DSC curves of S300 system are represented in Figure 6. This pattern of isothermal DSC curves was also observed in the isothermal thermograms of R30 and S30 systems (Supporting Information Fig. S2). Because the melting temperature of LCE was in the range of 120–140°C, the isothermal DSC scan temperatures were determined as 160–200°C. Below this range, the curing reaction is too slow. On the other hand, curings of LCE molecules proceeded too fast to monitor maximum cure rate above this temperature. The heat flow associated with maximum cure rate increased with increasing cure temperature. This fact demonstrated that the PANI nanospheres did not show any diffusion-barrier effect, when it was used as a curing agent. The cure rate was determined from the isothermal DSC thermograms using following equation:

$$\frac{d\alpha}{dt} = \frac{\frac{dH}{dt}}{H_{\text{com}}},$$

where $\alpha$ is the extent of cure, and $H_{\text{com}}$ is complete heat of cure obtained from dynamic scan using a heating rate of 10°C/min. The maximum cure rates in the various LCE/PANI systems are shown in Figure 7. The maximum cure rate increased with increasing cure temperature. This fact supports that PANI nanomaterials did not show a diffusion-barrier effect. The maximum cure rate of R30 was slightly higher than S30 and S300 at low temperatures. At higher cure temperatures, the maximum cure rates of LCE/PANI systems were almost identical. This means that the effect of PANI morphology on cure rate was significant at low temperatures, whereas it became insignificant with increasing cure temperature. The maximum cure rate of S30 was slightly higher than that of S300 at all cure temperatures because the curing reaction was facilitated around PANI nanospheres (S30) with higher surface area as elucidated from the dynamic DSC examination.

To obtain the degree of cure, the isothermal DSC curves were integrated and the partial areas as a function of time were normalized with respect to $H_{\text{com}}$. The reaction kinetics of DGE-DHAMS was extensively analyzed in the previous article.[30] It was revealed that the overall reaction kinetics and parameters were independent of isothermal DSC scan temperatures. Because the isothermal cure behaviors of LCE/PANI nanomaterial systems were predicted to follow the reaction pathway in the previous study, it is considered to be reasonable to calculate the reaction kinetics and parameters at one representative temperature (middle range).

Figure 8 presents the degree of cure for LCE/PANI systems cured at 180°C. The degree of cure increased quickly in the early stage of the cure reaction and approached to an asymptotic value in every system. In the early stage of the cure reaction, the degree of cure for R30 was higher than those of S30 and S300. This fact revealed that the PANI nanorods accelerated cure reaction more than PANI nanosphere due to the orientation of LCE molecules

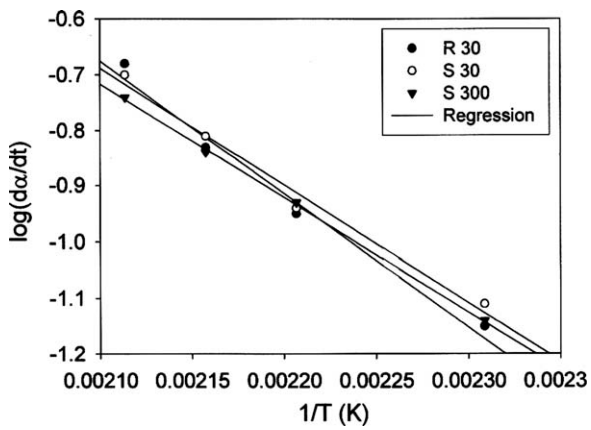


**Figure 7** Maximum cure rates of LCE/PANI systems.

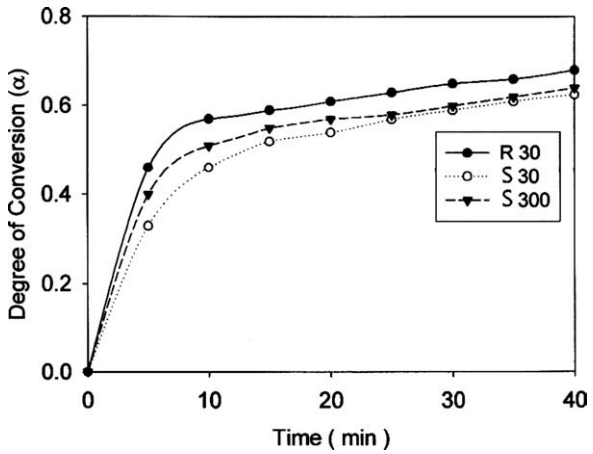


**Figure 8** Degree of cure of LCE/PANI systems cured at 180°C as a function of cure time.

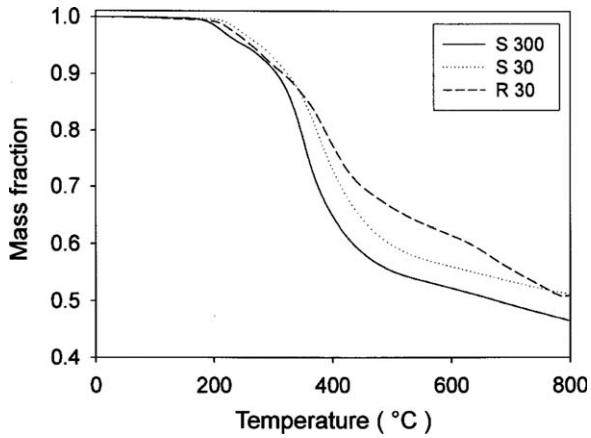


**Figure 9** TGA thermograms of LCE/PANI nanocomposites cured at 175°C for 3 h and at 190°C for 1 h.

around PANI nanorods in the early stage. As the reaction proceeded, the concentration of hydroxyl or amine groups generated from the breakage of epoxide groups increased and sufficient nucleophilic components existed. Therefore, cure rate became independent of PANI morphology in the middle of the cure reaction, because cure rate is mainly dependent on the concentration of nucleophilic components, which can participate in the curing reaction with electrophilic epoxide groups.[36] Accordingly, the final degree of cure was almost the same regardless of PANI type. This reaction can be denoted as an auto-catalyzed reaction. To prove that the cure reaction of LCE/PANI systems was an auto-catalyzed reaction, isothermal kinetic parameters were evaluated using the Kamal equation:[37]

$$d\alpha/dt = (k_1 + k_2 \times \alpha^m)(1 - \alpha)^n$$

where $k_1$ and $k_2$ are the kinetic rate constants, and $m$ and $n$ are kinetic exponents. This equation is valid for the auto-catalyzed reaction. The reaction parameters can be evaluated by the following way. First, the differential cure rate ($d\alpha/dt$) was obtained by normalization of cure enthalpy at fixed time to total cure enthalpy. Then the differential cure rate ($d\alpha/dt$) was integrated by summation in terms of time to obtain degree of cure at a fixed time. Thus, it is possible to collect data for degree of cure as a function of cure time. Finally, fitting by numerous iterations with above equation generated kinetic parameters. In the case of the R30 system, $m$ and $n$ values are 1.276 and 0.689, respectively. The $m + n$ value was 1.965, which was consistent with the general value (2) for the auto-catalyzed reaction.[38] For S30 and S300, the $m + n$ value was in the range of 1.5–1.9 depending on iteration accuracy. Isothermal DSC analysis verifies that PANI nanomaterials can be successfully used as curing agent and LCE/PANI systems showed general cure behavior of epoxy/amine system regardless of PANI morphology.

### Thermal and electrical properties

The thermal stability of cured LCE/PANI nanocomposites was investigated by thermogravimetric analysis (TGA) and illustrated in Figure 9. The TGA thermograms exhibited two weight loss regions, respectively. The first loss, started at around 250°C, was due to the initial degradation of less cross-linked epoxy network. The second weight loss region associated with the thermal degradation of the PANI component appeared at around 350°C. While the initial degradation temperature was almost the same regardless of PANI type, the second decomposition temperature was dependent on PANI morphology. Judging from this fact, it is inferred that the structural difference in LCE/PANI nanocomposites led to the different thermal stability. It has been reported that physical interaction between LCE molecules and PANI, which was generated from the addition of PANI nanofiller, cannot enhance the thermal resistivity of LCE network.[38] The second thermal decomposition temperature of R30 is higher than those of S30 and S300. On the other hand, thermal degradation temperature of S30 is slightly higher than that of S300. It is natural that increased surface area provided more reaction site. The curing reaction mainly happened on the surface of PANI nanomaterials. Curing reaction between the epoxide and amine groups on the surface of PANI nanomaterials resulted in the formation of strong covalent bond leading to improved thermal resistivity. Therefore, R30 with highest surface area had more chances for covalent bond formation, and thus enhanced thermal stability. In addition, R30 and S30 are more dispersive than S300 due to the nanoscale

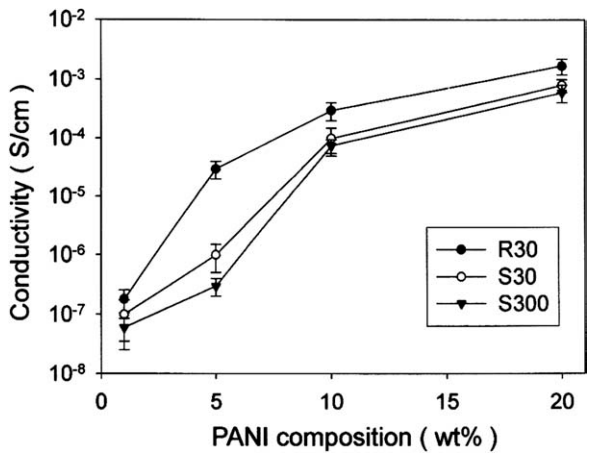


**Figure 10** Compositional effect for electrical conductivity of LCE/PANI nanocomposites cured at 175°C for 3 h and at 190°C for 1 h.

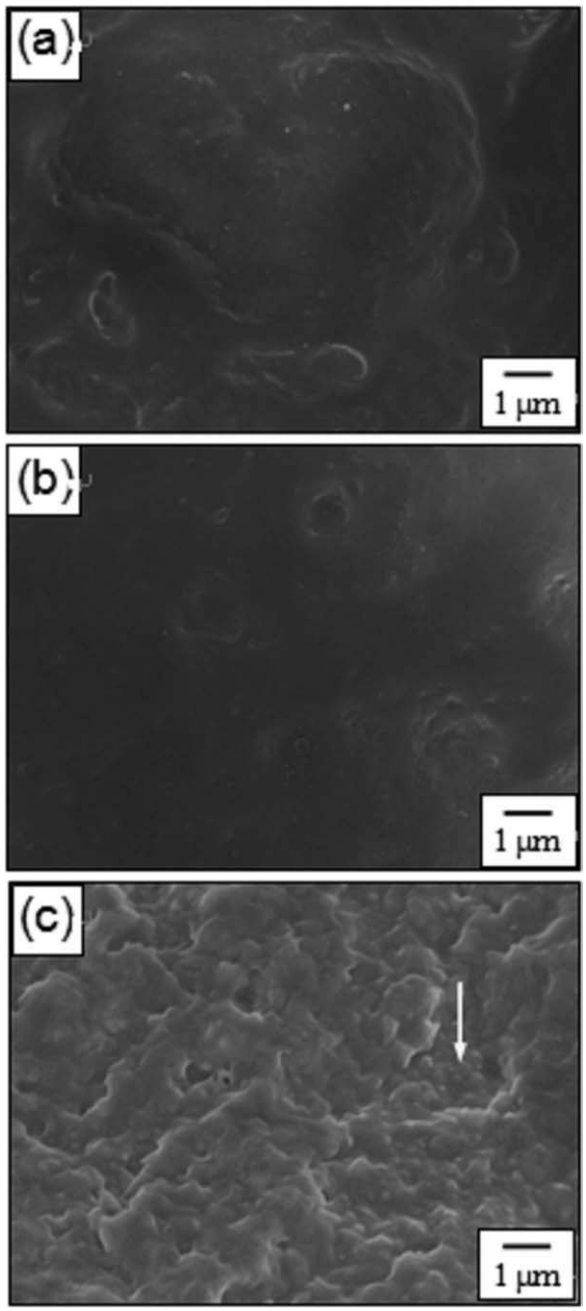


**Figure 11** SEM images of fracture surface of LCE/PANI nanocomposites cured at 175°C for 3 h and at 190°C for 1 h.

dimension.[29] For the case of R30, directional ordering of PANI nanorods in the LCE matrix might be induced during the cure reaction. This structural regularity also improved the thermal stability. The residual mass of LCE/PANI systems did not show a significant difference due to the similar degree of cure reaction.

The electrical conductivity of the prepared LCE/PANI nanocomposites measured by a standard four-probe method is exhibited in Figure 10 as a function of PANI composition. The electrical conductivity of LCE/PANI nanocomposites showed a percolation threshold behavior. This fact indicated that the electrical conductivity rose quickly at 5–10 wt %. It also means that more electrical paths were generated with increasing PANI concentration. In addition, the electrical conductivity of LCE/PANI nanocomposites was higher than conventional epoxy composite ($10^{-5}$–$10^{-4}$ S $cm^{-1}$).[39] This result confirmed that PANI nanomaterials can be used as novel conducting nanofillers. The electrical conductivity of R30 was higher than those of S30 and S300 at 5 wt %, and the R30 system showed a percolation threshold behavior at a lower PANI composition than S30 and S300, although there was no sharp transition region. This fact indicates that the R30 system can have sufficient electrical paths at a lower PANI composition. The morphological feature of PANI nanorods such as high aspect ratio induced an effect of generating more electrical paths.[40] Meanwhile, the electrical conductivity of S30 and S300 approached that of R30 above 10 wt% because of high inherent electrical conductivity of PANI.

### Fracture surface

The fracture surfaces of LCE/PANI nanocomposites were examined by SEM. Figure 11 demonstrates that the fracture surface of R30 and S30 was flat and homogeneous. On the contrary, the morphology of PANI particles of 300 nm was reflected regionally in the case of Figure 11(c). To prepare high performance LCE nanocomposites, homogeneous incorporation of filler into the matrix is very important. PANI nanomaterials have surface amine groups, which can form covalent bonds with LCE molecules. This covalent bond formation promoted dispersion of PANI nanomaterials into the LCE matrix, and thus prevented macrophase separation. Therefore, phase separation was not observed in the fracture surfaces of LCE/PANI nanocomposites [Figure 11(a–c)].

## CONCLUSIONS

The morphological effect of polyaniline nanomaterials on the cure behavior and performances of LCE/PANI nanocomposites was investigated. Dynamic DSC analysis indicated that PANI nanorods are more effective curing agent than PANI nanospheres below 25 wt % content, because PANI nanospheres retarded cure reaction toward the LCE matrix to some extent compared with PANI nanorods. Isothermal DSC study demonstrated that the degree of cure was almost independent of PANI nanoshape. TGA analysis and electrical conductivity of LCE/PANI nanocomposites revealed that the PANI nanomaterials could be effective as conducting fillers and advantageous for improving the performances of LCE/PANI nanocomposites.

## References


1. Giamberini, M.; Amendola, E.; Carfagna, C., Macromol Chem Phys 1997, 198, 3185.
2. Carfagna, C.; Acierno, D.; Palma, V. D.; Amendola, E.; Giamberini, M., Macromol Chem Phys 2000, 201, 2631.
3. Zhang, Y.; Vyazovkin, S., Macromol Chem Phys 2005, 206, 342.
4. Mormann, W.; Bröcher, M. Macromol Chem Phys 1996, 197, 1841.
5. Ribera, D.; Mantecón, A.; Serra, A., Macromol Chem Phys 2002, 202, 1658.
6. Ju, M.; Chen, M. Y.; Chang, F. C. Macromol Chem Phys 2000, 201, 2298.
7. Zerda, A. S.; Lesser, A. J. J Polym Sci Part B: Polym Phys 2001, 39, 1137.
8. Hsiue, G. H.; Liu, Y. L.; Liao, H. H. J Polym Sci Part A: Polym Chem 2001, 39, 986.
9. Barclay, G. G.; Ober, C. K.; Papathomas, K. I.; Wang, D. W. J Polym Sci Part A: Polym Chem 1992, 30, 1831.
10. Castell, P.; Serra, A.; Galia, M.; Giamberini, M.; Carfagna, C. J Polym Sci Part A: Polym Chem 2003, 41, 112.
11. Ng, S. C.; Ong, T. T.; Chan, H. S. O. J Mater Chem 1998, 8, 2663.
12. Jang, J.; Bae, J.; Yoon, S. H. J Mater Chem 2003, 13, 676.
13. Farren, C.; Akatsuka, M.; Takezawa, Y.; Itoh, Y. Polymer 2001, 42, 1507.
14. Tsotra, P.; Gryshchuk, O.; Friedrich, K. Macromol Chem Phys 2005, 206, 787.
15. Palaniappan, S.; Sreedhar, B.; Nair, S. M. Macromol Chem Phys 2001, 202, 1277.
16. Mu, S. Macromol Chem Phys 2005, 206, 689.
17. Yuan, G. L.; Kuramoto, N. Macromol Chem Phys 2004, 205, 1744.
18. González, I.; Vecino, M.; Muñoz, M. E.; Santamaría, A.; Pomposo, J. A. Macromol Chem Phys 2004, 205, 1379.
19. Jun, J. B.; Kim, J. W.; Suh, K. D. Macromol Chem Phys 2002, 203, 1011.
20. Oyaizu, K.; Mitsuhashi, F.; Tsuchida, E. Macromol Chem Phys 2002, 203, 1328.
21. Chen, Y.; Kang, E. T.; Neoh, K. G.; Huang, W. Langmuir 2001, 17, 7425.
22. Wei, Z.; Zhang, Z.; Wan, M. Langmuir 2002, 18, 917.
23. Huang, J.; Virji, S.; Weiller, B. H.; Kaner, R. B. J Am Chem Soc 2003, 125, 314.
24. Han, M. G.; Armes, S. P. Langmuir 2003, 19, 4523.
25. Gangopadhyay, R.; De, A. Chem Mater 2000, 12, 608.
26. Milo, S. P.; Windle, A. H. Adv Mater 1999, 11, 937.
27. Sue, H. J.; Earls, J. D.; Hefner, R. E., Jr. J Mater Sci 1997, 32, 4031.
28. Sue, H. J.; Earls, J. D.; Hefner, R. E., Jr.; Villarreal, M. I.; Garcia-Meitin, E. I.; Yang, P. C.; Plummer, C. J. G. Polymer 1998, 39, 4707.
29. Jang, J.; Oh, J. H.; Stucky, G. D. Angew Chem Int Ed 2002, 41, 4016.
30. Bae, J.; Jang, J.; Yoon, S. H. Macromol Chem Phys 2002, 203, 2196.
31. Ozawa, T. Bull Chem Sci (Japan) 1965, 38, 1881.
32. Ozawa, T. J Thermal Anal 1970, 2, 301.
33. Mallon, J. J.; Adams, P. M. Mol Cryst Liq Cryst 1991, 208, 65.
34. Mallon, J. J.; Adams, P. M. Mol Cryst Liq Cryst 1992, 213, 173.
35. Sreedhar, B.; Palaniappan, S.; Narayanan, S. Polym Adv Technol 2002, 13, 459.
36. Earls, J. D., Hefner, R. E., Jr., Puckett, P. M. U.S. Patent 5,218,062, 1993.
37. Kamal, M. R.; Sorour, S.; Ryan, S. M. Soc Plast Eng Tech Papers 1973, 19, 187.
38. Ishida, H.; Rodriguez, Y. The Preprints of the 35th IUPAC International Symposium on Macromolecules, Akron, Ohio, USA, July 1–15, 1994, p 634.
39. Sandler, J.; Shaffer, M. S. P.; Prasse, T.; Bauhofer, W.; Schulte, K.; Windle, A. H. Polymer 1999, 40, 5967.
40. Jang, J.; Yoon, H. Chem Commun 2003, 720.